Power Electronic Systems
Laboratory

IEEE Journal of Emerging and Selected Topics in Power Electronics, Vol. 12, No. 2, pp. 2333-2344, April 2024

Automatic Time-Division Multiplexing for Inductive Power Transfer to Multiple Stainless-Steel-Enclosed Receivers

J. Xu,
S. Miric,
D. Bortis,
M. Blickenstorfer,
M. Hitz,
J. W. Kolar,
J. Huber

ETH zürich

This article has been accepted for publication in IEEE Journal of Emerging and Selected Topics in Power Electronics. This is the author's version which has not been fully edited and content may change prior to final publication. Citation information: DOI 10.1109/JESTPE.2024.3350883

Automatic Time-Division Multiplexing for Inductive Power Transfer to Multiple Stainless-Steel-Enclosed Receivers

Junzhong Xu, *Member, IEEE*, Spasoje Mirić, *Member, IEEE*, Dominik Bortis, *Senior Member, IEEE*, Markus Blickenstorfer, Marco Hitz, and Johann W. Kolar, *Fellow, IEEE*, and Jonas Huber, *Senior Member, IEEE*

***Abstract*—Linear actuators employed in the food-processing or pharmaceutical industry must be enclosed in stainless steel (SS) for hygienic reasons. Therefore, cables and cable carriers should be avoided and wireless, i.e., inductive power transfer (IPT) should be employed. To achieve high efficiencies, the magnetic field components of the IPT system should be oriented parallel to the SS enclosures, which can be achieved with a coaxial arrangement of closed magnetic cores mounted on the moving part / slider and a stationary primary winding. As an alternative to the typically employed current-impressed operating modes of IPT systems with a constant primary-winding current that limits part-load efficiency, the high magnetic coupling of this arrangement facilitates operation as an isolated constant-voltage-transfer-ratio series-resonant dc-dc converter, i.e., a dc transformer (DCX). However, then, only a single receiver can receive power at any given time, and a time-division multiplexing (TDM) method is needed to supply multiple receivers with power in a cyclic manner. This paper proposes a novel automatic TDM (A-TDM) method that, unlike previous TDM methods, does not require any communication link nor a central controller. The new method is verified during startup, steady-state operation, and under load transients using an exemplary SS-enclosed IPT system with two 100 W receivers.**

***Index Terms*—Inductive power transfer, linear actuator, stainless-steel enclosure, multiple receivers, time-division multiplexing.**

I. Introduction

LINEAR motion is ubiquitous in a wide range of industrial applications. These include material handling tasks (e.g., pick-and-place) in high-purity environments such as food processing or pharmaceutical production facilities, which have to comply with high standards regarding hygiene and cleaning procedures and thus typically require all equipment, including linear actors, to be enclosed in stainless steel (SS) housings [1,2]. **Fig. 1** shows a state-of-the-art SS-enclosed linear actuator system. The relatively long stroke is handled best with the shown arrangement of a fixed stator containing permanent magnets and a coaxially arranged slider with the electrically supplied motor windings. Thus, an electrical connection to the moving slider is needed, also because it typically carries another task-specific actor or, in general, a powered tool. The corresponding supplying cables and cable carriers cannot be enclosed in SS, are therefore difficult to clean, and particles produced by wear and tear may contaminate the application processes. Therefore, cable-free alternatives, and, in particular, inductive power transfer (IPT) to the moving carriage would be advantageous [3].

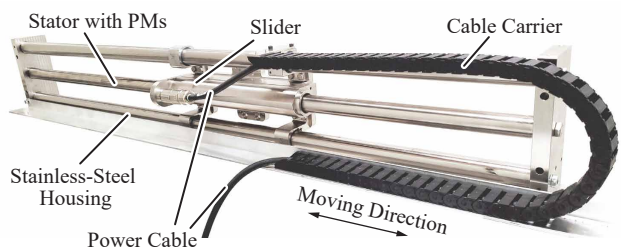

Fig. 1. State-of-the-art SS-enclosed linear actuator for high-purity environments. Note the fixed permanent-magnet-filled stator rod and the coaxially arranged moving slider carrying the motor windings, and the thus needed moving cables and cable carrier assembly, which cannot be enclosed in SS.

Since the 1990s, IPT for linear-motion applications has been suggested for mining applications [4], generic power delivery systems for mobile loads [5], and linear actuators [6]. IPT is also employed in industrial (monorail) transport systems [7] and for material-handling applications in general [8]. Similar IPT systems are further considered for roadway-powered electric vehicle concepts [9,10]. However, none of these applications requires SS enclosures.

As SS has a conductivity of about 1.3 MS/m, the alternating magnetic fields required for IPT induce eddy currents in SS enclosures, in particular if the magnetic field has significant components that penetrate the SS sheets orthogonally. These eddy currents, first, create a shielding effect according to Lenz's law and, for a given operating frequency, there is an upper limit to the feasible SS thickness (penetration/skin depth). Second, the eddy currents cause Joule heating (losses) in the SS enclosures, which degrades the IPT efficiency. Note that IPT for underwater (seawater) applications faces similar challenges [11,12]. Thus, systems for IPT through SS enclosures typically operate at low frequencies of only up to a few 100 Hz [13]–[17]. If thick SS layers (e.g., 10 mm in [14]) or metal boundaries with higher conductivity (e.g., aluminum in [18]) are involved, power levels of only a few watts and efficiencies of less than 50% are reported. On the other hand, [17] describes super-low-frequency (400 Hz) IPT through a 1 mm SS plate, achieving about 320 W of power transfer and an efficiency of 80%. Similarly, and as all examples so far, still using a geometric arrangement that

J. Xu, D. Bortis, J. W. Kolar, and J. Huber are with the Power Electronic Systems Laboratory, ETH Zurich, Switzerland.

S. Mirić is with the Drive and Energy System Laboratory, University of Innsbruck, Austria.

M. Blickenstorfer and M. Hitz are with NTI AG, Switzerland.

results in a major part of the magnetic field being perpendicular to the SS sheets, the authors have demonstrated IPT of 70 W through two 0.5 mm SS sheets (i.e., targeting the SS-enclosed linear-motion application discussed above) with an operating frequency of 2.25 kHz and an efficiency of about 71% [19].

Since the movement of the receivers considered here is constrained to a single dimension, and since no receivers need to be added or removed during operation, the IPT system can advantageously employ a *coaxial* arrangement of the transmitter and the receivers as shown in **Fig. 2a**. This approach is well known in applications without SS enclosures [4,11,20]. Since a closed magnetic core, carrying the secondary-side winding of a receiver, is coaxially sliding along a primary winding that extends over the full stroke of the linear actor, the resulting magnetic field is *tangential* (and not orthogonal) to the advantageously also coaxially arranged enclosures (i.e., SS pipes) [21]. Thus, the area available for the formation of eddy currents is limited by the thickness of the enclosures (typ. in the range of 0.1 mm to 0.5 mm) and hence very small; in the same way, eddy currents and/or losses in electric motors are limited by laminating the magnetic circuits exposed to ac flux. Note that a detailed discussion of the modeling of the eddy-current losses in and the temperature rise of the SS enclosures is beyond the scope of this paper, but is documented in [21].

The high magnetic coupling provided by the closed magnetic core allows to operate the IPT system like an isolated dc-dc converter with a well coupled high-frequency transformer. In particular, the dc transformer (DCX) concept [22]–[24] can be employed, i.e., the total series inductance L_s of the coaxial transformer arrangement (L_s is dominated by the loop inductance of the primary winding) can be compensated at the desired operating frequency f_s with a series capacitor $C_r = (4\pi^2 f_s^2 L_s)^{-1}$ (see **Fig. 2b**); the DCX then achieves a constant and (almost) load-independent voltage transfer ratio and/or output voltage in open-loop operation and thus without the need for a communication channel. Moreover, the magnetizing current facilitates zero-voltage switching (ZVS) of the primary-side inverter's transistors. Note further that the DCX operates in a voltage-impressed manner, i.e., the primary-side inverter generates a fixed rectangular ac voltage u_p and the primary-winding current i_p adapts to the load. In [21], we have thus demonstrated that such an IPT-through-SS system can achieve significantly better performance than earlier concepts: specifically, transferring 100 W through two 0.5 mm-thick SS enclosures at an operating frequency of 20 kHz and an efficiency of 97% is feasible.

In typical linear-motion applications there is often a need to provide more than just a single carriage (mover, slider) per linear actor. Consequently, the IPT system should allow to operate multiple receivers, as illustrated in **Fig. 2a**. However, each secondary-side winding magnetically couples to the same shared primary winding. Thus, the equivalent load impedances of the secondaries are reflected to the primary side and appear as a series connection (see also **Fig. 2b**), i.e., the total primary-side voltage is shared among all connected receivers. To still maintain constant output voltages regardless of the number of connected receivers or the power they draw (i.e., their effective load impedances), the input voltage must increase

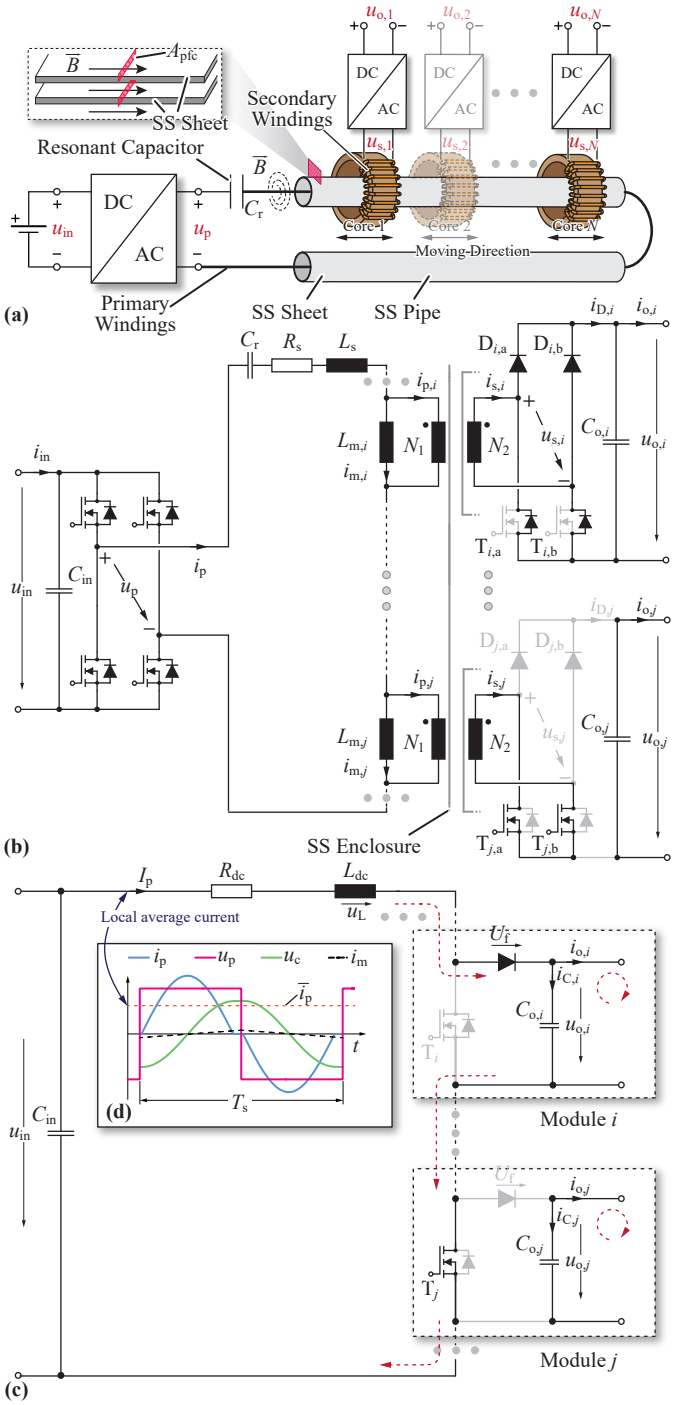

Fig. 2. IPT system with multiple receiver modules. **(a)** Conceptual physical arrangement and **(b)** power circuit where only one receiver is connected to the ac link (its transistors are off). **(c)** Dynamic dc-dc equivalent circuit representation of the power circuit from (b). **(d)** Key waveforms illustrating the relationship between the dc current in the equivalent circuit and the ac current in the real converter, i.e., $I_p = \bar{i}_p$.

or decrease accordingly. Thus, the required behavior at the input of the primary winding corresponds to that of a current source with a current level defined by the highest secondary-side load. Therefore, the most prominent realization option for IPT systems with multiple receivers (with coaxial or other configuration of the magnetic circuit) is to use a current-impressed mode of operation [4,11,25]–[32]. To achieve this,

the primary-side inverter can be actively controlled to maintain a constant current i_p in the primary winding. Further, to limit the required dc input voltage (essentially defined by the sum of all receiver voltages reflected to the primary side), often an LCL compensation network is connected between the primary-side inverter and the primary winding to provide voltage-to-current conversion (the required high voltage then appears across the LCL network's capacitor, but not at the inverter terminals, i.e., the LCL network's input) [26,27,30]. Each receiver can control its own output voltage by repeatedly short-circuiting its (secondary-side) winding, which essentially decouples the receiver from the primary-side winding, resulting in zero power flow [26]. As the primary-side current is impressed, the other receivers are not affected and hence there is typically no need for a communication channel between the primary-side and the individual receivers. Many variants of this core concept have been proposed, e.g., based on the quantum approach [33], or on adjusting the phase angle and/or the magnitude of the receivers' input voltages, which also facilitates bidirectional power flow [27,34,35]. Note that even though—for reasons of energy conversion—the power delivered by the primary-side inverter adapts to the total power consumed by all receivers, the current in the primary winding does not, i.e., it is independent of the momentary load situation and typically set to cover the maximum rated load of any receiver output. Given the typically long primary winding with a thus large series resistance R_s, this significantly degrades the efficiency in part-load situations. Therefore, concepts to adapt the primary-winding current to the total load have been studied, e.g., using sliding-mode control, [33]. Also, power management approaches where the connection and disconnection of the receivers is coordinated (which requires communication, for example via the IPT frequency) such that the primary-side current does not have to be as high as needed for providing rated power to the receivers, have been discussed [29]. At any point in time, however, the primary-side current is defined by the receiver with the maximum instantaneous load, not by the total / average load of all receivers combined.

Therefore, the voltage-impressed operating mode with its inherently load-dependent primary winding current seems interesting [36], especially for applications with loads that show a high ratio of peak to average power as is typical for linear actors. As indicated above, the resulting interactions between the receivers prevent the voltage-impressed operating mode if more than one receiver should be connected *at the same time*. Thus, [37] proposed a time-division multiplexing (TDM) method to supply two receivers (each tuned to a different resonant frequency) from one primary; by changing the ratio at which the primary operates at the first and at the second resonant frequency, the power transfer to the two receivers can be adjusted individually. In [38], the TDM concept is employed with a single operating frequency and a central controller is used to coordinate the receivers such that at any given time only one receiver couples to the primary, i.e., communication between the central controller and each receiver is needed. Similarly, we have analyzed the suitability of such a TDM concept (with a single operating frequency) for the considered application of SS-enclosed linear actuators (which typically show a high ratio of peak to average power and hence favor concepts with potentially high part-load efficiency) in [21], and [39] provides a quantitative comparison of current-impressed and voltage-impressed operation of SS-enclosed IPT systems with multiple receivers.

TABLE I
KEY PARAMETERS OF THE CONSIDERED EXAMPLE SYSTEM WITH A TRACK LENGTH OF $L_{track} = 82\,\text{cm}$.

Symbol	Parameter	Value
U_{in}	Rated input voltage	72 V
$P_{o,r}$	Rated output power	100 W
C_o	Output capacitance	260 µF
f_s	Switching frequency	20 kHz
f_r	Resonant frequency	20.6 kHz
C_r	Compensation capacitor	200 nF
$L_{m,i}$	Magnetizing inductance	12 mH
$N_1 : N_2$	Turns ratio	16:16
R_s	Lumped series resistance	1.6 Ω
L_s	Lumped series inductance	300 µH
U_f	Lumped diode voltage drop	1.37 V

The implementation of the TDM concept (which will be discussed in detail below) is relatively straightforward if a communication link between all units (primary-side inverter, all receivers) is available. However, whereas such a link may exist in specific applications, self-sufficiency is still a desirable feature of a power supply system, i.e., the IPT system should have the capability of standalone operation without the need for a dedicated communication link (note that the current-impressed options discussed above do so intrinsically). In this paper, we therefore propose an *automatic* TDM (A-TDM) method for multi-receiver IPT systems using the voltage-impressed DCX mode of operation. The method achieves TDM, i.e., the mutually exclusive supply of each receiver in a cyclic manner and fully autonomous output voltage control for each receiver, without any communication link.

In the following, first **Section II** describes the system modeling and the desired ideal TDM behavior in detail. **Section III** then introduces the proposed A-TDM method and **Section IV** provides extensive experimental verification before **Section V** concludes the paper.

II. Ideal Time-Division Multiplexing

As discussed above, TDM operation allows to retain the DCX operating mode in closely-coupled IPT systems with multiple receivers by always only connecting a single receiver at a time, and thus supply power to the receivers in a cyclic manner. The relative connection time of each receiver depends on both, its own power consumption and the total (average) power consumption of all receivers. Before presenting the proposed A-TDM method, it is useful to describe first the desired, i.e., ideal behavior.

Consider an IPT system with N_r receivers, each with rated output power $P_{o,r}$ and nominal output voltage $U_{o,r}$. The dc input voltage U_{in} of the primary-side inverter is constant. **Fig. 2a** shows the conceptual arrangement and **Fig. 2b** shows the electrical power circuit. Note further that R_s and L_s represent, for simplicity reasons, the lumped series resistance and series inductance of the primary loop and one connected receiver; both

This article has been accepted for publication in IEEE Journal of Emerging and Selected Topics in Power Electronics. This is the author's version which has not been fully edited and content may change prior to final publication. Citation information: DOI 10.1109/JESTPE.2024.3350883

are typically dominated by the primary loop alone. C_r is the series resonant capacitor that compensates L_s at the operating frequency to facilitate DCX operation. **Tab. I** lists the key parameters of the example system considered throughout the paper. Note that a unity turns ratio (i.e., $N_1 = N_2$) is considered as a result of equal input and output voltages. Therefore, we use primary-side and secondary-side quantities interchangeably without explicitly accounting for the turns ratio.

As TDM operation requires each receiver to be able to decouple itself from the ac link, the receivers feature a semi-bridge-less active rectifier (SAR): by gating on the two transistors, a receiver can short-circuit its secondary-side winding, rendering it essentially transparent to the rest of the IPT system. Thus, each receiver can be in either of two states: CONNECTED (its transistors $\mathrm{T_i}$ are off) or DISCONNECTED (its transistors $\mathrm{T_i}$ are on). Out of the N_r receivers, only one single receiver is in the CONNECTED state at any given time. Handovers of the CONNECTED state from one receiver to the next are allowed after complete switching periods. Thus, a TDM period T_tdm is an integer multiple of the switching period: $T_\mathrm{tdm} = N_\mathrm{tdm} T_\mathrm{s}$ with $N_\mathrm{tdm} \geq N_\mathrm{r}$, i.e., during a complete cycle, each receiver is connected at least during one switching period. Selecting longer T_tdm values thus increases the granularity of the power delivery to the different receivers.

For the further analysis, it is useful to consider a dynamic equivalent circuit of the DCX that accurately captures its terminal behavior. Based on [23,24], **Fig. 2c** shows the dynamic equivalent circuit corresponding to the power circuit from **Fig. 2b**, where $R_\mathrm{dc} = \pi^2/8 \cdot R_\mathrm{s}$ and $L_\mathrm{dc} = \pi^2/4 \cdot L_\mathrm{s}$. Together with $I_\mathrm{p} = \bar{i}_\mathrm{p}$ (i.e., a dc current corresponding to the local average value of the actual primary current flows in the equivalent circuit; the magnetizing current is neglected), this ensures that the equivalent circuit has equal load-dependent losses and equal load-dependent stored energy as the real circuit; both is needed to correctly capture the terminal behavior [24].

Ideally, the primary-side inverter delivers a constant power, which corresponds to the sum of all receivers' power consumption (plus losses), i.e., neglecting losses, the maximum input power delivered by the inverter becomes $P_\mathrm{in,r} = N_\mathrm{r} P_\mathrm{o,r}$. Thus, the constant input dc voltage and a given operating point (characterized by a certain load distribution among the receivers) result in a non-varying primary current $I_\mathrm{p} = const.$ (i.e., a dc current in the equivalent circuit, corresponding to a constant amplitude of the resonant current pulses in the real circuit). Of course, I_p adapts to the total load supplied, (i.e., to changing operating points), which is in contrast to the current-impressed systems discussed earlier. Given a non-varying I_p, the series voltage drop across R_s and the diodes of the connected receiver is constant, too: $\Delta v_\mathrm{s} = I_\mathrm{p} R_\mathrm{dc} + U_\mathrm{f}$ (whereby U_f approximates the diode forward voltage drops with constant value). Correspondingly, the losses in these series elements are $P_\mathrm{s} = I_\mathrm{p}^2 R_\mathrm{dc} + I_\mathrm{p} U_\mathrm{f}$. Because of the I_p^2 term, $I_\mathrm{p} = const.$ results in minimum losses. Ideally, the output voltage of each connected receiver thus settles at $U_\mathrm{o} = U_\mathrm{in} - \Delta v_\mathrm{s} = const.$ (neglecting the system dynamics).

The *instantaneous* power available for a connected receiver is $I_\mathrm{p} U_\mathrm{o}$, and in addition

$$I_\mathrm{p} U_\mathrm{o} = \sum_{i=1}^{N_\mathrm{r}} P_{\mathrm{o},i} \tag{1}$$

must hold, where, $P_{\mathrm{o},i}$ denotes the *average* output power of a receiver. However, a receiver is not always connected but only during a certain *share* of T_tdm. To provide the required average output power $P_{\mathrm{o},i}$ for receiver i, we must have

$$P_{\mathrm{o},i} = \frac{t_{\mathrm{conn},i}}{T_\mathrm{tdm}} I_\mathrm{p} U_\mathrm{o} = D_i I_\mathrm{p} U_\mathrm{o} \tag{2}$$

and thus the duty ratio becomes

$$D_i = \frac{P_{\mathrm{o},i}}{\sum_{i=1}^{N_\mathrm{r}} P_{\mathrm{o},i}} \quad \text{with} \quad \sum D_i = 1. \tag{3}$$

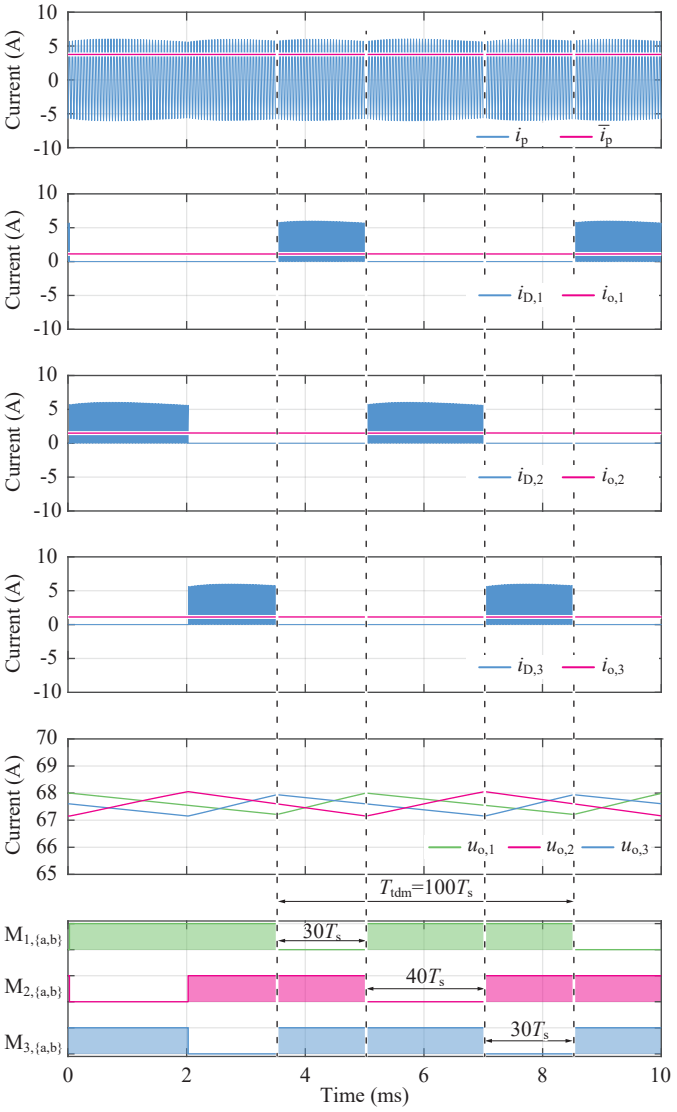

Fig. 3. Simulated key waveforms of idealized TDM operation with three receivers ($P_{\mathrm{o},1}$ = 75 W, $P_{\mathrm{o},2}$ = 100 W, and $P_{\mathrm{o},3}$ = 75 W); **Tab. I** gives the system specifications, but a larger C_o = 5 mF has been used to limit the impact of the converter dynamics at the handovers for illustration purposes. During a TDM period of $T_\mathrm{tdm} = 100 T_\mathrm{s}$, each receiver is connected to the ac link (and hence receives power) only during a fraction that corresponds to its share of the total load supplied by all receivers, see (3); the output voltages are (in average) equal ($U_{\mathrm{o},1} = U_{\mathrm{o},2} = U_{\mathrm{o},3} \approx 67.5$ V.)

This article has been accepted for publication in IEEE Journal of Emerging and Selected Topics in Power Electronics. This is the author's version which has not been fully edited and content may change prior to final publication. Citation information: DOI 10.1109/JESTPE.2024.3350883

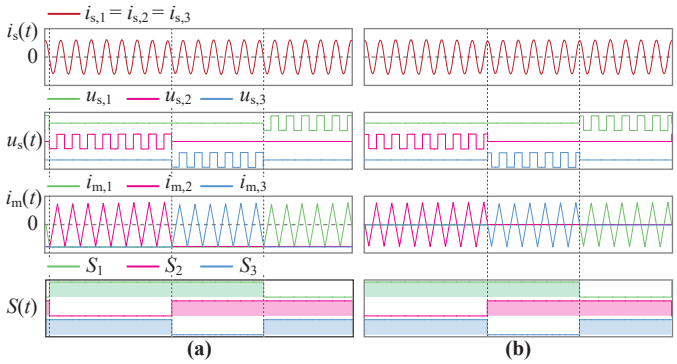

Fig. 4. Simulated waveforms of idealized TDM operation with three receivers when the transistors switch **(a)** when the resonant current crosses zero or **(b)** when the resonant current attains its peak (i.e., in the center of a resonant pulse), which advantageously prevents offsets in the magnetizing currents, $i_{m,i}$.

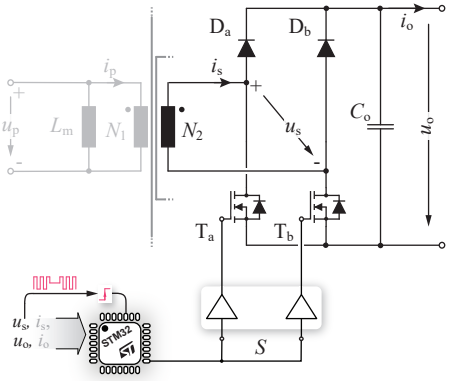

Fig. 5. Conceptual implementation of the proposed A-TDM on a receiver module with the sensed power quantities indicated. Synchronization of a local carrier wave to the inverter output voltage is achieved using the zero-crossings of the ac-side voltage u_s (which can be sensed in the CONNECTED state with $S = 0$, i.e., turned-off transistors).

Finally, in practical applications the output voltage ripple should be limited, e.g., to $\delta u_{o,pp} = \Delta u_{o,pp}/U_o = 10\,\%$. This voltage ripple can (assuming piecewise linear behavior, i.e., assuming constant output current, etc.) be expressed as

$$\Delta u_{o,pp} = (1 - D_i) \cdot T_{tdm} \cdot \frac{P_{o,i}}{C_o U_o}. \tag{4}$$

The worst case occurs for the combination of maximum power and longest disconnection interval, i.e., when all N_r receivers operate with full load, i.e., $P_{o,i} = P_{o,r}\ \forall\ i$. Then, $D_i = 1/N_r$ and we have

$$C_o = \frac{P_{o,r}}{\delta u_{o,pp} U_o^2} \cdot \left(1 - \frac{1}{N_r}\right) \cdot T_{tdm} \tag{5}$$

for a given T_{tdm}. Considering the minimum $T_{tdm} = N_r T_s$ mentioned above, the minimum required capacitance is

$$C_o \geq \frac{P_{o,r}}{\delta u_{o,pp} U_o^2} \cdot (N_r - 1) \cdot T_s. \tag{6}$$

Note that typically $T_{tdm} > N_r T_s$ is used to improve the resolution of D_i. Furthermore, especially if high efficiency is targeted (i.e., smooth I_p as discussed above), it is desirable to limit the voltage ripple to very low values as the corresponding voltage difference determines the transient response of the dynamic equivalent circuit after handover from one receiver to the next; then, however, relatively large capacitors are needed.

The simulation results shown in **Fig. 3** illustrate the ideal TDM behavior for an exemplary operating point with three receivers and a fixed $T_{tdm} = 100 T_s$. Note how the different loads are mapped to different durations of the power transfer to the individual receivers, i.e., to the duty cycles D_i. The primary-side winding current i_p features an essentially constant amplitude (some minor dynamics resulting from the handovers are visible; these will be explained in more detail below).

As an aside, note that there are two different ways of aligning the receivers' state transitions with the switching periods. As indicated in **Fig. 4a**, the receivers' transistors can be switched at a zero crossing of the resonant current. However, then, the core remains magnetized when a receiver enters the DISCONNECTED state (i.e., only demagnetizes very slowly with the low voltage drop of the two transistors), which over time may lead to saturation issues. It is therefore advantageous to shift the state transitions by $\pi/2$, i.e., to align them with the center of a resonant pulse as shown in **Fig. 4b**. At these instants, the core is, ideally, demagnetized. On the other hand, the switching transitions occur at the peak current and hence the switching losses increase, which, however, is acceptable given the relatively low repetition rate of the state transitions (as we typically have $T_{tdm} \gg T_s$).

III. Automatic Time-Division Multiplexing

All in all, ideal TDM operation clearly requires a central coordination as (3) implies that no receiver can calculate its duty cycle without knowing the power consumption of the others, and also a synchronization of the link access must be ensured. To eliminate the thus needed dedicated communication channels, an automatic TDM (A-TDM) strategy is proposed in this section, which only utilizes power quantities that each receiver can measure and process independently to achieve the desired TDM behavior; i.e., there is no central controller. Specifically, the quantities that each receiver measures are the output voltage, u_o, and the ac-side input voltage, u_s, as indicated in **Fig. 5**. Furthermore, optionally also the output current i_o and/or the ac-side current i_s can be measured for protection purposes, and, in case of i_s, to improve the performance. The A-TDM functionality is best described with finite state machines (FSMs). After an initial discussion of the synchronization mechanism (**Section III-A**), **Section III-B** first discusses normal operation and **Section III-C** describes an advanced technique to reduce the primary rms current, before finally **Section III-D** presents the startup procedure.

A. Synchronization

As indicated above, a receiver's mode transitions should be synchronized to the inverter's output voltage (or, equivalently, the resonant current), which serves as a common time base for all receivers. Whereas using the ac current for synchronization has the advantage that the information is available to a receiver regardless of its state (CONNECTED or DISCONNECTED), a (comparably expensive) current sensor would be needed, and, at low power, noise and limited accuracy may lead to unreliable

This article has been accepted for publication in IEEE Journal of Emerging and Selected Topics in Power Electronics. This is the author's version which has not been fully edited and content may change prior to final publication. Citation information: DOI 10.1109/JESTPE.2024.3350883

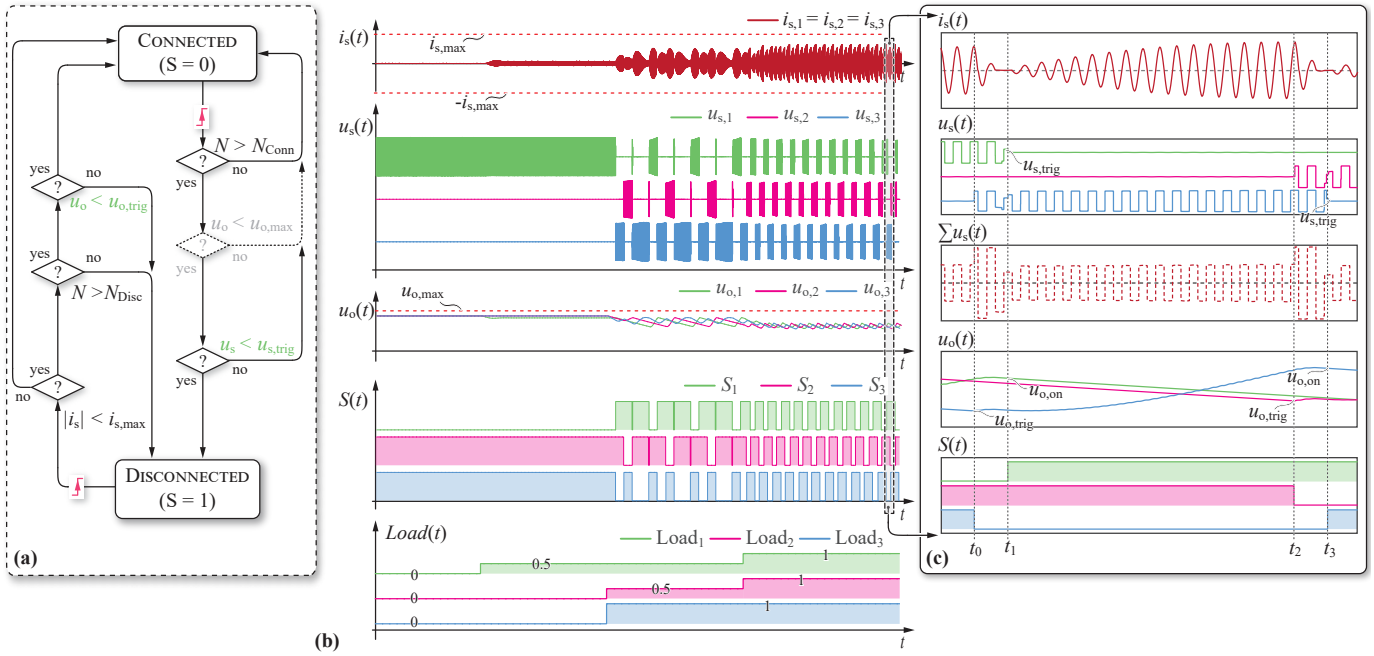

Fig. 6. Proposed A-TDM operation. **(a)** FSM running on each receiver module to control its transitions between the two states CONNECTED (transistors are off) and DISCONNECTED (transistors are on); the receiver module measures its dc output voltage u_o, the ac-side current i_s and the ac-side voltage u_s. **(b)** Conceptual waveforms for A-TDM operation with three receivers and changing load conditions (0%, 50%, 100%), and **(c)** zoomed view used for the detailed explanation (see text) of the handover process from receiver 1 to receiver 3.

zero-crossing detection. Therefore, the zero crossings of the ac voltage u_s (see **Fig. 5**) are used to synchronize the phase and the frequency of a local carrier wave. Note that when the receiver is disconnected (i.e., the transistors are turned on), $u_s \approx 0 = const.$ and hence the synchronization signal is not available. This, however, is not an issue because of the fixed operating frequency and the opportunity to update the synchronization information at least during a few switching cycles (where the receiver is in the CONNECTED state) in each TDM period.

B. Normal A-TDM Operation

In steady-state operation, the finite state machine (FSM) shown in **Fig. 6a** controls a receiver's behavior, i.e., the transitions between the two states: CONNECTED with the transistors turned off (S = 0) or DISCONNECTED with the transistors turned on (S = 1). Using the synchronized local carrier, each receiver evaluates possible state transitions once in every switching half-period, i.e., advantageously in the middle of a switching half-period (see **Fig. 4b**); this is indicated by the trigger symbols in the FSM diagram.

The key idea of the A-TDM method is that a connected receiver can detect the presence of a second connected receiver by measuring the ac input voltage, u_s, which reduces to $u_s = u_p/N_r$ once the resonant current decays to zero and the receivers' diodes stop conducting. The details are best explained using a specific example, i.e., the handover from receiver 1 to receiver 3 shown in **Fig. 6c** between $t = t_0$ and $t = t_1$:

- $t < t_0$: Receiver 1 is CONNECTED and receivers 2 and 3 are DISCONNECTED. Thus, receiver 1 draws power from the primary side in DCX mode to charge its output capacitor and supply its load. On the other hand, the output voltages of the other receivers reduce as they supply power to their loads.
- $t = t_0$: The output voltage of receiver 3 reaches a lower threshold value, $u_{o,3} = u_{o,trig}$. This threshold value is calculated upon entering the DISCONNECTED state based on the measured output voltage and the specified maximum relative peak-to-peak output voltage ripple, i.e., $u_{o,trig} = u_{o,Disc} \cdot (1 - \delta u_{o,pp})$. It is not sensible to select an absolute value, as the average output voltage depends on the total system load because of the load-dependent voltage drop across the primary winding's resistance, see **Section II**. There should be, however, a hard minimum value $u_{o,trig,min} > u_{s,trig}$ to prevent too low output voltages that would then not allow a receiver to remain in the CONNECTED state (as the condition $u_s < u_{s,trig}$ would be true even while only one receiver is connected). If furthermore the receiver has been disconnected for at least N_{Disc} switching half-periods[1], receiver 3 transitions to the CONNECTED state, too.
- $t_0 < t < t_1$: *Two* receivers are connected and thus, considering the equivalent circuit from **Fig. 2c**, the resonant current is quickly driven to zero as $u_{o,1}+u_{o,3} \approx 2U_o \gg U_{in}$. Once the resonant current subsides, the ac input voltages of the two receivers are $u_{s,1} \approx u_{s,3} \approx u_p/2$. In particular, for receiver 1, the condition $u_{s,1} < u_{s,trig}$ becomes true (the threshold value $u_{s,trig}$ is selected slightly higher than $u_p/2$ or $U_{in}/2$), and hence it transitions to the DISCONNECTED state at $t = t_1$.

[1]This mechanism ensures that once a receiver disconnects, it stays disconnected for a certain minimum time, thus preventing a premature triggering of a next handover.

This article has been accepted for publication in IEEE Journal of Emerging and Selected Topics in Power Electronics. This is the author's version which has not been fully edited and content may change prior to final publication. Citation information: DOI 10.1109/JESTPE.2024.3350883

- $t > t_1$: Finally, the handover is completed and receiver 1 is DISCONNECTED while receiver 3 is CONNECTED.

Likewise, the next handover from receiver 3 to receiver 2 occurs between t_2 and t_3.

In addition to those mentioned above, the FSM shown in **Fig. 6a** contains a few more conditions that influence the state transitions. Specifically, a transition from DISCONNECTED to CONNECTED is immediately triggered if the measured current peak value i_s exceeds a maximum allowable value, i.e., if $i_s > i_{s,max}$. This behavior serves as a protection mechanism against corner cases where, e.g., all receivers disconnect, or the connected receiver fails in a way that short-circuits its input, and hence the primary current quickly increases.

Similarly, the condition $u_o < u_{o,max}$ does not allow a receiver to transition from the CONNECTED to the DISCONNECTED state if its output voltage is too high. As long as a receiver remains connected, the output voltage cannot further increase due to the limited input voltage U_{in}. On the other hand, if the receiver disconnects, potentially the situation described in the previous paragraph could arise, i.e., all receivers might end up in the DISCONNECTED state. The primary current amplitude then quickly increases until all receivers, including the receiver with too high output voltage, are forced to the CONNECT state again. The current then decays within a few switching periods, but those pulses still transfer energy to all receivers, potentially further increasing the output voltages.

Further, to handle race conditions (e.g., two receivers entering the CONNECTED state at the same time), a transition from CONNECTED to DISCONNECTED is only possible if the receiver has been connected for at least N_{Conn} half cycles, where N_{Conn} is a random number. To illustrate how the use of a random value for N_{Conn} advantageously contributes to handling race conditions, assume that receiver 1 is CONNECTED, and then receiver 2 and receiver 3 enter the CONNECTED state *at the same time*. Receiver 1 then quickly detects the presence of other CONNECTED receivers and immediately disconnects ($u_s < u_{s,trig}$ is true). Then, receiver 2 and receiver 3 both are connected, and thus the condition $u_s < u_{s,trig}$ remains true for both of them. If N_{Conn} was *not* a random number, both receivers would enter the DISCONNECTED state at the same time, resulting in a situation where *all* three receivers are disconnected and hence the primary current would quickly increase. Ultimately, the condition $i_s > i_{s,max}$ becomes true—but again for all three receivers at the same time. Thus, all would enter the CONNECTED state at the same time, starting a vicious cycle from which there is no escape. In contrast, with N_{Conn} being a random number, i.e., different for each receiver, even if receiver 2 and receiver 3 enter the CONNECTED state at the same time, one of them would transition back to DISCONNECTED state earlier than the other, thus restoring normal A-TDM operation with only one receiver in the CONNECTED state. The random N_{Conn} should be selected within an interval whose lower bound depends on the minimum time needed to bring the maximum resonant current to zero, because only then a CONNECTED receiver can detect the presence of one (or more) other CONNECTED receivers.

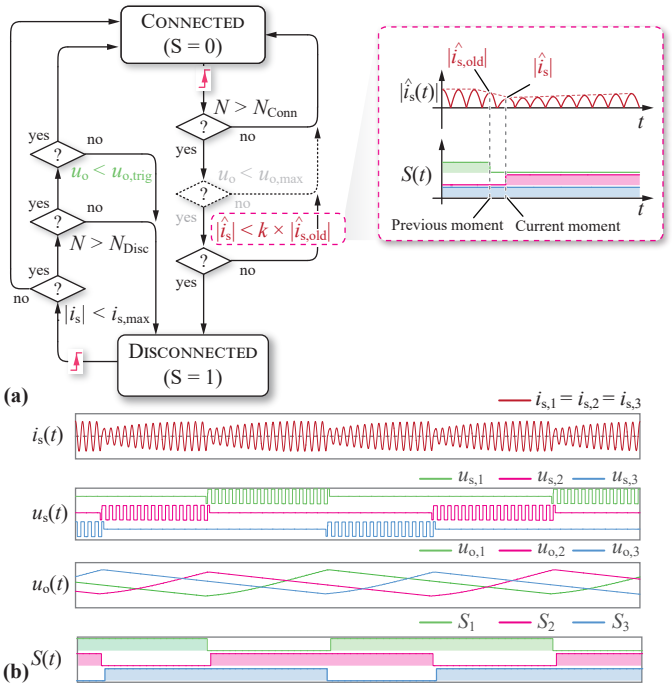

Fig. 7. A-TDM operation with reduced rms current (compared to **Fig. 6**). **(a)** Correspondingly modified FSM that utilizes the difference between two subsequent resonant current pulse amplitudes to detect when a second receiver connects; the receiver module measures its dc output voltage u_o, the ac-side current i_s and the ac-side voltage u_s. **(b)** Simulated waveforms for three receivers with full load; note that unlike to the case shwon in **Fig. 6b**, the primary current does not reduce to zero during the handovers.

Thus,

$$N_{Conn,min} = \left\lceil \frac{L_{dc} I_{p,max}}{2U_o - U_{in}} \cdot \frac{2}{T_s} \right\rceil. \tag{7}$$

The upper bound is given by the maximum time that one receiver can remain connected before another receiver would require power when all receivers operate with rated load, i.e.,

$$N_{Conn,max} = \left\lfloor \frac{\delta u_{o,pp} U_o^2 C_o}{(N_r - 1)\, P_{o,r}} \cdot \frac{2}{T_s} \right\rfloor. \tag{8}$$

In this way, the FSM from **Fig. 6a** realizes A-TDM operation of multiple receivers with variable loads without any communication link. However, as the implemented signalling utilizes the secondary-side ac voltage measurements, it necessarily requires the ac current to subside to zero at each handover. Only then the ac voltage reduces to $u_s \approx u_p/2$ (if two receivers are connected at the same time), but this results in "notches" in the primary current envelope (see **Fig. 6b**). These, and the finite dynamics of the current amplitude reaching the steady-state value again after a handover, increase the primary current rms value above that observed for the ideal TDM operation.

C. Normal/Steady-State Operation with Reduced RMS Current

This behavior can be improved if the receivers are equipped with a current sensor measuring their ac input current, specifically the peak values of the sinusoidal current pulses (remember that the execution of the recevier's state machine is synchronized and aligned such that it occurs in the center

This article has been accepted for publication in IEEE Journal of Emerging and Selected Topics in Power Electronics. This is the author's version which has not been fully edited and content may change prior to final publication. Citation information: DOI 10.1109/JESTPE.2024.3350883

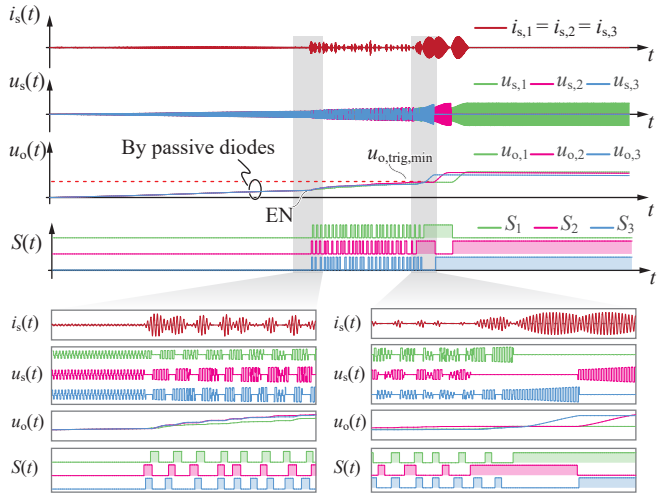

Fig. 8. Simulated startup behavior. After an initial passive charging phase, the receivers' controllers start and, using same FSM as for normal operation (see **Fig. 6**), further charge their output capacitors to the nominal output voltage.

of each switching/resonant half period). As indicated in the alternative FSM for the NORMAL state shown in **Fig. 7a**, a CONNECTED receiver can then utilize the difference between the peak values of two subsequent current pulses to detect the presence of a second CONNECTED receiver.

Specifically, as discussed above and considering the equivalent circuit from **Fig. 2c**, when *two* receivers are connected at the same time, a large negative voltage appears across L_{dc} because $2U_o \gg U_{in}$. This quickly reduces the current i_s, i.e., leads to large differences between subsequent peak values of the resonant current. The reduction can be described by a factor $k = |\hat{i}_s|/|\hat{i}_{s,old}|$, such that the condition for transitioning to the DISCONNECTED state can be expressed as $|\hat{i}_s| < k \cdot |\hat{i}_{s,old}|$ (instead of $u_s < u_{s,trig}$ before). Advantageously, detecting this condition does *not* require the current to decay to zero (for the diodes to stop conducting), and hence quicker handovers with less pronounced "notches" in the primary current can be achieved, as is illustrated by the simulated waveforms in **Fig. 7b**.

Note that also a load shedding of a receiver, i.e., its load reducing instantaneously from 100% to 0%, leads to a quick decay of the current amplitudes as the receiver's dc-link capacitor voltage increases. However, this process is necessarily much slower (due to the presence of the dc-link capacitor) compared to the case of interest where a second receiver connects and thus the total effective secondary-side voltage immediately doubles. Therefore, it is possible to select k such that the two cases can be clearly distinguished.

In practice, this mode works best for higher power levels, where noise in the current measurement becomes irrelevant compared to the amplitude differences; for low power, the voltage-based method is preferable (note also that the impact of the rms current reduction on the system losses becomes more important with increasing power).

D. Startup

Advantageously, the FSM shown in **Fig. 6** also facilitates startup of the system, which is described based on the simulation results shown in **Fig. 8**. Initially, the output capacitors of all receivers are fully discharged. Correspondingly, the receivers' controllers are not active and hence only the passive diode rectifier functionality is available. To limit the inrush current, the primary-side inverter thus ramps up the duty cycle of its output voltage from zero to 100% while the receivers' output capacitors charge via the passive diode rectifiers to (approximately) U_{in}/N_r. This voltage must suffice for the receiver's auxiliary power supplies to power up and supply the local control hardware.

At this point, all receivers are in the CONNECTED state and hence synchronization of the local carrier to the zero crossings of the ac voltage u_s is possible as described in **Section III-A**. Once powered up and synchronized, the FSM brings the receivers to the DISCONNECTED state because $u_s < u_{s,trig}$, which is always true due to the still low output voltages (i.e., $u_o < u_{s,trig}$). Note that for fully identical receivers and perfect symmetry, this would happen at the same time for all receivers. In practice, this is not the case but still the receivers must be assumed to power up in rapid succession, i.e., several receivers might start counting the cycles in the CONNECTED states for evaluating the condition $N > N_{Conn}$ (to disconnect) at the same time. This corresponds to the race condition described above in **Section III-B** and the mechanism described there, based on selecting N_{Conn} randomly (within certain bounds), ultimately results in time intervals where only one receiver is connected, allowing it to further charge its output capacitor until $U_o > u_{o,trig,min}$. Finally, once all receivers achieve this, A-TDM operation continues as discussed in the preceding sections.

IV. Experimental Verification

The industrial linear actuator prototype shown in **Fig. 9a** is used to validate the proposed A-TDM method. We have described the optimization of the IPT hardware itself (i.e., the primary-side inverter, the resonant tank, SS losses, etc.) in [21], and **Tab. I** summarizes the key specifications. Here, the system is configured with two receivers, i.e., two sliders, each carrying a drive inverter for the corresponding motor windings and a second linear motor (again including a drive inverter) oriented in the z direction as an exemplary load.

Fig. 9b shows the hardware prototype of a receiver module, whose power stage realizes $T_{a,b}$ with Infineon IPB073N15N5 silicon MOSFETs driven by NCP8104 gate drive ICs, and the diodes $D_{a,b}$ are Rohm RB218NS150 silicon Schottky diodes (two in parallel). Furthermore, there is an isolated dc-dc converter (PDQE15-D) to provide auxiliary power for the drive inverters on the 24 V level in addition to the main 72 V power output. The control algorithms are implemented on an STM32G431 ARM microcontroller unit (MCU). Both, the ac input voltage u_s and the output dc voltage u_o are measured using the MCU's onboard ADCs. In addition, an external AD8612 comparator is used to implement the fast zero-crossing detection of u_s needed for synchronization. To retain full flexibility for testing different operating modes, the prototype also features sensors (LEM GO-SME-10) for the ac and dc currents; in a final application, one or both might be eliminated for cost reasons. Further, **Tab. II** summarizes

This article has been accepted for publication in IEEE Journal of Emerging and Selected Topics in Power Electronics. This is the author's version which has not been fully edited and content may change prior to final publication. Citation information: DOI 10.1109/JESTPE.2024.3350883

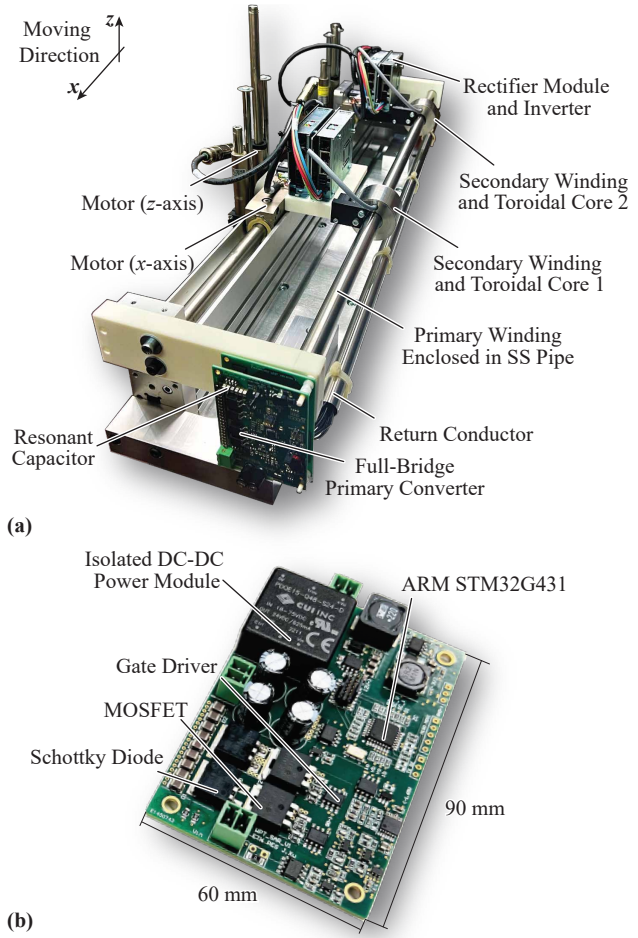

Fig. 9. **(a)** Industrial linear actor prototype with two sliders, each carrying an IPT receiver, the motor inverter, and a second actuator (z-direction) with its drive. The length of the track is 82 cm. Note that the relevant parts (i.e., the primary winding as well as two secondary-side core/winding assemblies) are fully enclosed in 0.5 mm SS sheets. **(b)** Close-up of the 100 W IPT receiver module PCB (see the power circuit in **Fig. 5**).

TABLE II
FSM (SEE **FIG. 6** AND **FIG. 7**) PARAMETERS USED FOR THE EXPERIMENTS.

Symbol	Parameter	Value
N_{Disc}	Min. no. half-cycles DISCONNECTED	2
$N_{\text{Conn,min}}$	Min. no. half-cycles CONNECTED (lower bound)	4
$N_{\text{Conn,max}}$	Min. no. half-cycles CONNECTED (upper bound)	20
$u_{\text{o,trig,min}}$	Min. output voltage threshold	55 V
$u_{\text{s,trig}}$	Multi-receiver presence detection threshold	40 V
$u_{\text{o,max}}$	Max. output voltage limit	75 V
$i_{\text{s,max}}$	Max. ac peak current limit	15 A
$\delta u_{\text{o,pp}}$	Max. relative output voltage peak-to-peak ripple	10%
k	RMS reduction algorithm parameter	0.8

the configuration parameters of the FSMs implementing the A-TDM method (see **Section III** and, in particular, **Fig. 6a** and **Fig. 7a** for details). In the following, the demonstrator operates under characteristic conditions (startup, steady-state, load steps) with the two receivers loaded by resistors instead of the motor drives, which facilitates defined operating points.

A. Startup

Fig. 10a shows measured key waveforms of the system startup, where both receivers are loaded with a 2 kΩ resistor. After an initial phase of passive charging via the diode rectifiers, the MCUs power up (note that this does not happen at the same time due to tolerances in the hardware). As described in **Section III-D**, the output voltages then increase to the nominal values, whereby the FSMs' state transitions are governed by N_{Disc} and the (random[2]) N_{Conn}, which results in frequent handovers. Finally, normal A-TDM operation continues with approximately equal duty cycles due to the equal (though very low) loads and, given the target output voltage ripple of about 10%, with a much lower handover frequency.

B. Continuous Operation and Load Steps

Figs. 10b-d show key waveforms of the demonstrator from **Fig. 9** with two receivers (with resistive loads) and the proposed A-TDM operation for a typical use case where receiver 2 operates with full load ($P_{\text{o,2}}$ = 100 W) while receiver 1 is subject to three different load steps, i.e., from no load to full load (**Fig. 10b**), from full load to half load (**Fig. 10c**), and from full load to no load (**Fig. 10d**), respectively. Note how the duty cycles of the two receivers (i.e., the relative time each stays in the CONNECTED state) adapt to the changing load scenarios. Furthermore, the zoomed view in **Fig. 10b** shows that the rms current reduction method introduced in **Section III-C** works as intended, i.e., the primary-side current does not subside to zero during the handovers. This algorithm is only activated for $i_{\text{s}} \geq 2$ A, and therefore is not enabled in the right part of **Figs. 10cd** (and the zoomed views there). Clearly, the proposed A-TDM implementation achieves regulated output voltages of both receivers in steady-state and also during the load transients, while the measured waveforms closely match the simulation results presented earlier.

C. Efficiency

Fig. 11 shows the measured efficiencies and rms currents for operation with and without the rms current reduction method from **Section III-C** activated for higher loads, where a corresponding improvement of the efficiency can be observed. Note further that the peak efficiency of 88.2% (both receivers at 50% load) is relatively low and, in the demonstrator, limited by the relatively high resistance (R_{s} = 1.6 Ω) of the primary winding, which is realized from solid wires for economic reasons.

V. CONCLUSION

This paper proposes an automatic time-division multiplexing (A-TDM) method for wireless power transfer (IPT) to multiple receivers using a voltage-impressed operating mode without the need for a load-independent current in the primary winding, which facilitates improved part-load efficiency, and without an LCL-type compensation network on the primary side, which reduces the implementation effort. On the other hand, TDM

[2]Pseudo-random numbers are generated using the `rand()` function from the C standard library.

This article has been accepted for publication in IEEE Journal of Emerging and Selected Topics in Power Electronics. This is the author's version which has not been fully edited and content may change prior to final publication. Citation information: DOI 10.1109/JESTPE.2024.3350883

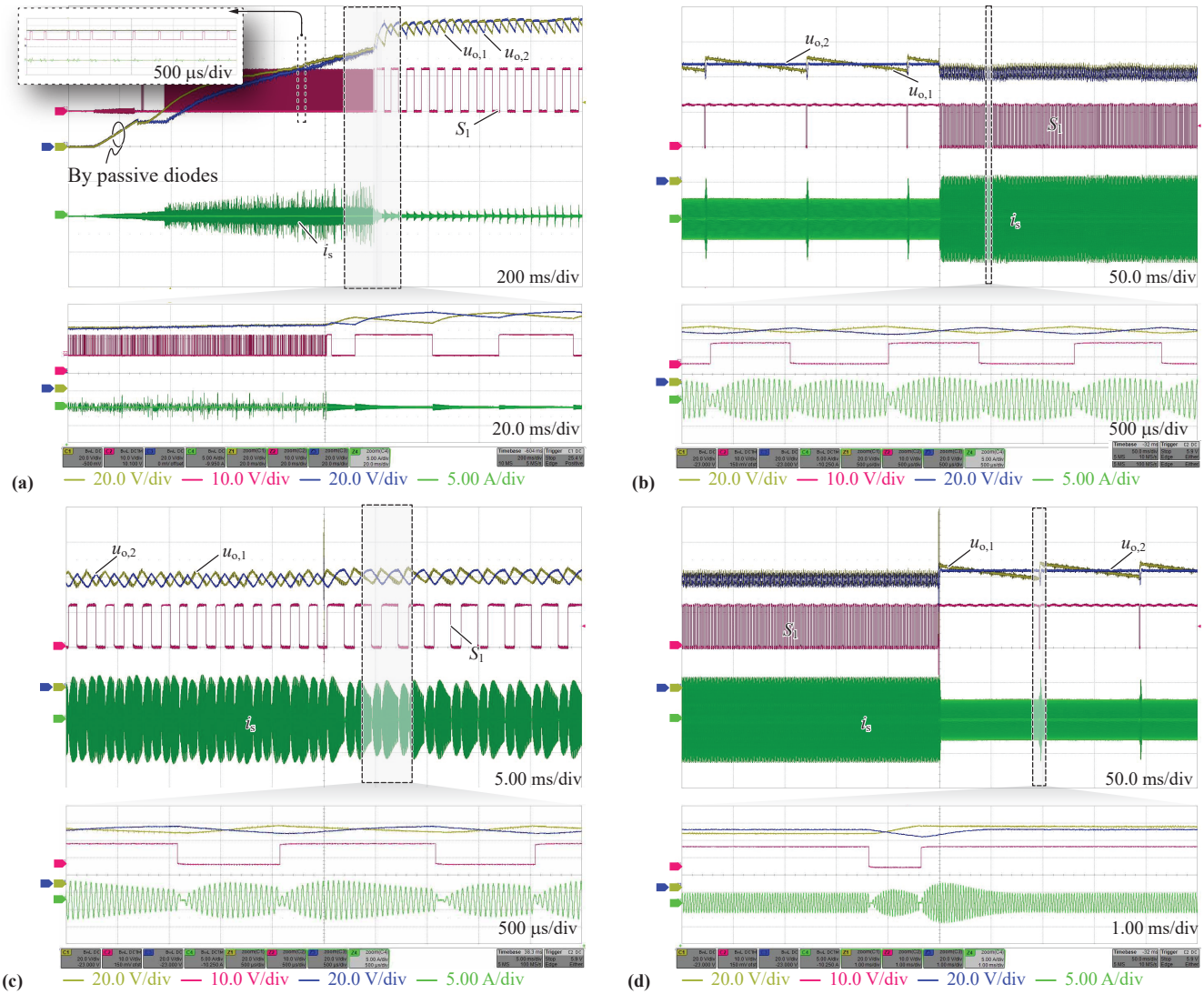

Fig. 10. Measured key waveforms of the demonstrator from **Fig. 9** with two receivers (and resistive load) using the proposed A-TDM operation: output voltages $u_{o,1}$ (yellow) and $u_{o,2}$ (blue), gate signal S_1 of receiver 1's transistors (red), and receiver 1's ac input current $i_{s,1}$ (green), which essentially equals the primary winding current. **(a)** Startup with light load (2 kΩ resistive load). **(b)** to **(d)** show A-TDM operation under different load scenarios with step transitions in between: while receiver 2 always operates with full load (100 W), receiver 1 is subject to various load-steps, i.e., **(b)** from 0% to 100%, **(c)** from 100% to 50%, and **(d)** from 100% to 0%. Note how both dc output voltages are maintained equal (in average) and close to the nominal value.

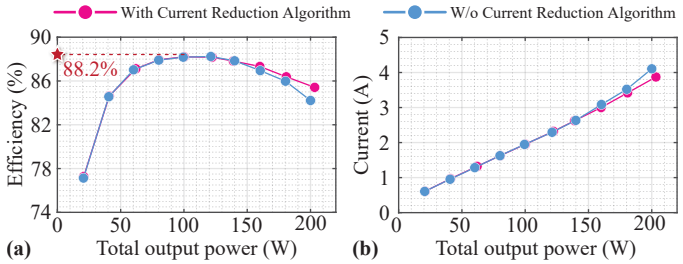

Fig. 11. **(a)** Measured (Yokogawa WT1804E) efficiencies and **(b)** primary-side rms current of the demonstrator from **Fig. 9** with two receivers. Both receivers are loaded equally, i.e., $P_{o,1} = P_{o,2}$ for each measurement point. Note the reduction of the rms current and a corresponding efficiency improvement at high loads if the improved handover method from **Section III-C** is enabled.

operation is required, i.e., the mutually exclusive power transfer to each receiver in a cyclic manner, which, in contrast to previous work, here is achieved without any communication link between the receivers and without a central controller. Instead, the finite state machine (FSM) controlling a receiver's behavior does so solely using measurements of power quantities (voltages and currents) available to each receiver anyway. The proposed A-TDM method is experimentally verified during startup, steady-state, and transient (load steps) operation using a stainless-steel-enclosed IPT system with two 100 W receivers. Whereas simulation results show that the proposed A-TDM method successfully works with three receivers, too, a detailed analysis of the method's scalability to higher receiver counts could be targeted by future research.

Acknowledgements

This work was supported by Innosuisse, for which the authors are most grateful. J. Xu would further like to thank the Shanghai Jiao Tong University (SJTU) for the funding of his research fellowship at the Power Electronic Systems Laboratory of ETH Zurich.

References

[1] A. Zaske and S. Halverson, "Top 5 best practices for designing electric actuators into food processing equipment," 2020. [Online]. Available: https://www.tolomatic.com/info-center/resource-details/top-5-best-practices-for-designing-electric-actuators-into-food-processing-equipment/

[2] G. Lyon, "Linear motion design for washdown applications," 2019. [Online]. Available: https://pages.pbclinear.com/rs/909-BFY-775/images/White-Paper-Linear-Motion-Design-in-Washdown.pdf

[3] R. Christen, U. Fischli, T. Franz, M. Schueller, and J. Smajic, "Wireless power transfer system for linear drives," in *Proc. 23rd Int. Conf. Comput. Electromagn. Fields (COMPUMAG)*, Cancun, Mexico, Jan. 2022.

[4] K. W. Klontz, D. M. Divan, D. W. Novotny, and R. D. Lorenz, "Contactless power delivery system for mining applications," *IEEE Trans. Ind. Appl.*, vol. 31, no. 1, pp. 27–35, 1995.

[5] J. Barnard, J. Ferreira, and J. van Wyk, "Sliding transformers for linear contactless power delivery," *IEEE Trans. Ind. Electron.*, vol. 44, no. 6, pp. 774–779, Dec. 1997.

[6] K. I. Woo, H. S. Park, Y. H. Cho, and K. H. Kim, "Contactless energy transmission system for linear servo motor," *IEEE Trans. Mag.*, vol. 41, no. 5, pp. 1596–1599, May 2005.

[7] Daifuku Co., Ltd., "Non-contact power supply transport system technology," 2001. [Online]. Available: https://www.daifuku.com/solution/technology/wirelesspower/

[8] G. A. Covic and J. T. Boys, "Inductive power transfer," *Proc. IEEE*, vol. 101, no. 6, pp. 1276–1289, Jun. 2013.

[9] S. Y. Choi, B. W. Gu, S. Y. Jeong, and C. T. Rim, "Advances in wireless power transfer systems for roadway-powered electric vehicles," *IEEE Trans. Emerg. Sel. Topics Power Electron.*, vol. 3, no. 1, pp. 18–36, Mar. 2015.

[10] C. C. Mi, G. Buja, S. Y. Choi, and C. T. Rim, "Modern advances in wireless power transfer systems for roadway powered electric vehicles," *IEEE Trans. Ind. Electron.*, vol. 63, no. 10, pp. 6533–6545, Oct. 2016.

[11] B. Heeres, D. Novotny, D. Divan, and R. Lorenz, "Contactless underwater power delivery," in *Proc. Power Electron. Spec. Conf. (PESC)*, Taipei, Taiwan, 1994, pp. 418–423.

[12] A. Askari, R. Stark, J. Curran, D. Rule, and K. Lin, "Underwater wireless power transfer," in *Proc. IEEE Wireless Power Transfer Conf. (WPTC)*, Boulder, CO, USA, May 2015.

[13] O. Imoru, A. Jassal, H. Polinder, E. Nieuwkoop, J. Tsado, and A. A. Jimoh, "An inductive power transfer through metal object," in *Proc. 1st Int. Future Energy Electron. Conf. (IFEEC)*, Tainan, Taiwan, Nov. 2013, pp. 246–251.

[14] M. Yamakawa, Y. Mizuno, J. Ishida, K. Komurasaki, and H. Koizumi, "Wireless power transmission into a space enclosed by metal walls using magnetic resonance coupling," *Wireless Engin. Technol.*, vol. 5, no. 1, pp. 19–24, 2014.

[15] D.-X. Yang, Z. Hu, H. Zhao, H.-F. Hu, Y.-Z. Sun, and B.-J. Hou, "Through-metal-wall power delivery and data transmission for enclosed sensors: A review," *Sensors*, vol. 15, no. 12, pp. 31 581–31 605, Dec. 2015.

[16] H. Zhang, L. Ding, N. Liu, F. Yang, and L. Qian, "Optimal operating frequency of inductive power transfer through metal barriers," in *Proc. 89th IEEE Vehicular Technol. Conf. (VTC)*, Kuala Lumpur, Malaysia, Apr. 2019.

[17] H. Ishida, T. Kyoden, and H. Furukawa, "Super-low-frequency wireless power transfer with lightweight coils for passing through a stainless steel plate," *Rev. Sci. Instrum.*, vol. 89, no. 3, Mar. 2018.

[18] T. A. Vu, C. V. Pham, A.-V. Pham, and C. S. Gardner, "Wireless power transfer through metal using inductive link," *Int. J. Power Electron. Drive Syst.*, vol. 10, no. 4, pp. 1906–1913, Dec. 2019.

[19] S. Mirić, M. Tatić, J. Huber, D. Bortis, and J. W. Kolar, ""Pushing power through walls" – Wireless power transfer through stainless steel," in *Proc. 24th IEEE Int. Conf. Electr. Machines Syst. (ICEMS)*, Gyeongju, Korea, Nov. 2021, pp. 743–751.

[20] K. Moriki, A. Kawamura, T. Shimono, T. Nozaki, K. Ikeda, J. Sato, H. Hayashiya, and H. Yamamoto, "Technological feasibility of coaxial contactless power transmission for traction power supply," in *Proc. 16th Int. Power Electron. Motion Contr. Conf. Expo. (PEMC)*, Antalya, Turkey, Sep. 2014, pp. 967–972.

[21] S. Mirić, J. Xu, J. Huber, D. Bortis, M. Hitz, and J. W. Kolar, "Wireless power supply of moving linear actuator enclosed in stainless-steel," in *Proc. Wireless Power Week (WPW)*, Bordeaux, France, 2022, pp. 354–360.

[22] W. McMurray, "The thyristor electronic transformer: A power converter using a high-frequency link," *IEEE Trans. Ind. Gen. A.*, vol. IGA-7, no. 4, pp. 451–457, Jul. 1971.

[23] A. Esser and H.-C. Skudelny, "A new approach to power supplies for robots," *IEEE Trans. Ind. Appl.*, vol. 27, no. 5, pp. 872–875, 1991.

[24] J. E. Huber, J. Miniböck, and J. W. Kolar, "Generic derivation of dynamic model for half-cycle DCM series resonant converters," *IEEE Trans. Power Electron.*, vol. 33, no. 1, pp. 4–7, 2017.

[25] A. Kelley and W. Owens, "Connectorless power supply for an aircraft-passenger entertainment system," *IEEE Trans. Power Electron.*, vol. 4, no. 3, pp. 348–354, Jul. 1989.

[26] J. Boys, G. Covic, and A. Green, "Stability and control of inductively coupled power transfer systems," *IEE Proc. El. Power Appl.*, vol. 147, no. 1, pp. 37–43, 2000.

[27] U. K. Madawala and D. J. Thrimawithana, "A bidirectional inductive power interface for electric vehicles in V2G systems," *IEEE Trans. Ind. Electron.*, vol. 58, no. 10, pp. 4789–4796, Oct. 2011.

[28] Z. Pantic, S. Bai, and S. M. Lukic, "ZCS LCC-compensated resonant inverter for inductive-power-transfer application," *IEEE Trans. Ind. Electron.*, vol. 58, no. 8, pp. 3500–3510, Aug. 2011.

[29] L. J. Chen, J. T. Boys, and G. A. Covic, "Power management for multiple-pickup IPT systems in materials handling applications," *IEEE Trans. Emerg. Sel. Topics Power Electron.*, vol. 3, no. 1, pp. 163–176, Mar. 2015.

[30] J. Gottschlich, M. Schäfer, M. Neubert, and R. W. De Doncker, "A galvanically isolated gate driver with low coupling capacitance for medium voltage SiC MOSFETs," in *Proc. 18th Europ. Conf. Power Electron. Appl. (EPE/ECCE Europe)*, Karlsruhe, Germany, Sep. 2016.

[31] N. Yan, D. Dong, and R. Burgos, "A multichannel high-frequency current link based isolated auxiliary power supply for medium-voltage applications," *IEEE Trans. Power Electron.*, vol. 37, no. 1, pp. 674–686, Jan. 2022.

[32] P. Jayathurathnage, S. Mirić, J. Xu, J. Huber, , M. Hitz, J. Kyyrä, and J. W. Kolar, "New concept for current-impressed WPT to multiple independent stainless-steel-enclosed linear actuator sliders," in *Proc. IEEE Southern Power Electron. Conf. (SPEC)*, Nadi, Fiji, 2022.

[33] F. F. A. van der Pijl, M. Castilla, and P. Bauer, "Adaptive sliding-mode control for a multiple-user inductive power transfer system without need for communication," *IEEE Trans. Ind. Electron*, vol. 60, no. 1, pp. 271–279, Jan. 2013.

[34] X. Dai, J. Wu, J. Jiang, R. Gao, and U. K. Madawala, "An energy injection method to improve power transfer capability of bidirectional WPT system with multiple pickups," *IEEE Trans. Power Electron.*, vol. 36, no. 5, pp. 5095–5107, May 2021.

[35] L. Zhou, S. Liu, Y. Li, R. Mai, Y. Li, L. Fu, and L. Qi, "Efficiency optimization of LCC-S compensated multiple-receiver bidirectional WPT system for stackers in automated storage and retrieval systems," *IEEE Trans. Power Electron.*, vol. 37, no. 12, pp. 15 693–15 705, Dec. 2022.

[36] J. G. Meins and J. D. Sinsley, "Method and apparatus for supplying contactless power," U.S. Patent 6 515 878B1, Feb., 2003.

[37] C. Jiang, K. T. Chau, T. W. Ching, C. Liu, and W. Han, "Time-division multiplexing wireless power transfer for separately excited DC motor drives," *IEEE Trans. Magn.*, vol. 53, no. 11, Nov. 2017.

[38] W. Cai, D. Ma, X. Lai, K. Hashmi, H. Tang, and J. Xu, "Time-sharing control strategy for multiple-receiver wireless power transfer systems," *Energies*, vol. 13, no. 3, p. 599, Jan. 2020.

[39] J. Xu, S. Miric, M. Blickenstorfer, M. Hitz, J. W. Kolar, and J. Huber, "Comparative evaluation of voltage- and current-impressed inductive power transfer to multiple stainless-steel-enclosed moving receivers," in *Proc. Appl. Power Electron. Conf. Expo. (APEC)*, Long Beach, CA, USA, Feb. 2024.